Optimized simultaneous transverse and longitudinal focusing of intense ion beam pulses for warm dense matter applications

Adam B. Sefkow[a],*, Ronald C. Davidson[a], Igor D. Kaganovich[a], Erik P. Gilson[a], Prabir K. Roy[b], Peter A. Seidl[b], Simon S. Yu[b], Dale R. Welch[c], David V. Rose[c], John J. Barnard[d]

[a]*Plasma Physics Laboratory, Princeton University, Princeton, NJ 08543, USA*
[b]*Lawrence Berkeley National Laboratory, Berkeley, CA 94720, USA*
[c]*Voss Scientific, Albuquerque, NM 87108, USA*
[d]*Lawrence Livermore National Laboratory, Livermore, CA 94550, USA*

Available online 22 February 2007

Abstract

Intense, space-charge-dominated ion beam pulses for warm dense matter and heavy ion fusion applications must undergo simultaneous transverse and longitudinal bunch compression in order to meet the requisite beam intensities desired at the target. The longitudinal compression of an ion bunch is achieved by imposing an initial axial velocity tilt on the drifting beam and subsequently neutralizing its space-charge and current in a drift region filled with high-density plasma. The Neutralized Drift Compression Experiment (NDCX) at Lawrence Berkeley National Laboratory has measured a sixty-fold longitudinal current compression of an intense ion beam with pulse duration of a few nanoseconds, in agreement with simulations and theory. A strong solenoid is modeled near the end of the drift region in order to transversely focus the beam to a sub-millimeter spot size coincident with the longitudinal focal plane. The charge and current neutralization provided by the background plasma is critical in determining the total achievable transverse and longitudinal compression of the beam pulse. Numerical simulations show that the current density of an NDCX ion beam can be compressed over a few meters by factors greater than 10^5 with peak beam density in excess of 10^{14} cm^{-3}. The peak beam density sets a lower bound on the local plasma density required near the focal plane for optimal beam compression, since the simulations show stagnation of the compression when $n_{beam} > n_{plasma}$. Beam–plasma interactions can also have a deleterious effect on the compression physics and lead to the formation of nonlinear wave excitations in the plasma. Simulations that optimize designs for the simultaneous transverse and longitudinal focusing of an NDCX ion beam for future warm dense matter experiments are discussed.
© 2007 Elsevier B.V. All rights reserved.

1. Introduction

Heavy ion drivers for warm dense matter and heavy ion fusion applications can deliver more intensity to the target per unit length of accelerator by greatly compressing the intense ion charge bunches over short distances. Intense ion beams can be compressed to high current densities by transverse focusing to final diameters less than a few millimeters and longitudinal focusing to pulse durations of a few nanoseconds [1,2]. Optimizing the compression under the appropriate experimental constraints allows more compact and cost-effective accelerators and transport lines to be used as heavy ion drivers.

The majority of the ion beam's space-charge and current must be neutralized during the final transport stage [3,4] in order to overcome the defocusing self-field forces and achieve small spot size with short pulse duration. Simulations [5,6] and experiments [7–9] have shown that a high-density plasma satisfying $n_b \ll n_p$, where n_b and n_p are respectively the beam and plasma densities, provides sufficient charge and current neutralization during final

*Corresponding author.
E-mail address:* asefkow@pppl.gov (A.B. Sefkow).

transport for an intense ion beam to be transversely focused to a final radius of about 1 mm. Longitudinal compression is achieved by applying a time-dependent velocity tilt to the charge bunch and subsequently allowing it to drift through a neutralizing background plasma [10]. The velocity tilt is imposed on the ion beam by a single-gap linear induction accelerator [11] which employs a time-dependent voltage waveform. The Neutralized Drift Compression Experiment (NDCX) [12,13] at Lawrence Berkeley National Laboratory has measured the sixty-fold longitudinal compression in current [14] of an intense ion beam with pulse duration of a few ns, in agreement with simulations [15] and theory [16].

Theoretical techniques used to investigate the dynamical evolution of a compressing charge bunch propagating through a background plasma include warm-fluid [17], kinetic [18], hybrid fluid-Vlasov [16], and particle-in-cell (PIC) models [10,15]. The models show very good agreement with experimental data and provide physical insights into imperfections such as non-ideal velocity tilts, partial beam neutralization and residual space-charge effects, consequences of finite acceleration gap size, and beam temperature effects, all of which give rise to decreased compression factors and increased pulse widths at focus. A comparison between the measurement of longitudinal bunch compression in the NDCX device and the corresponding predicted amount of compression calculated by the LSP PIC simulation, kinetic model, and hybrid fluid-Vlasov model is shown in Fig. 1 [16]. This particular implementation of the kinetic model does not include a finite acceleration gap or non-ideal velocity tilt.

Presently, the transverse and longitudinal compression of intense ion beams have been separately demonstrated in experiments. However, simultaneous transverse and longitudinal focusing to a common focal plane is desired in order to maximize the amount of current density on the target for a given amount of initial beam charge. The goal for upcoming experiments on the NDCX device is to demonstrate the feasibility of simultaneous transverse and

longitudinal compression of an intense ion beam for warm dense matter and heavy ion fusion applications [19,20].

This paper is organized as follows. An optimized simulation using NDCX-relevant parameters for simultaneous transverse and longitudinal focusing, provided by a strong final-focus solenoid and the application of an axial velocity tilt, respectively, of an intense ion beam pulse is presented in Section 2. Section 3 provides a comparison of simultaneous focusing results under a variety of circumstances involving variations in the background plasma and final-focus solenoid parameters. Beam–plasma interaction simulations near the focal plane in the presence of a background magnetic field are described in Section 4. A brief summary and discussion of results are provided in Section 5.

2. Simulations of simultaneous focus

A powerful computational tool for self-consistently incorporating many effects of beam propagation through a background plasma is provided by particle-in-cell (PIC) simulations. The LSP [21,22] PIC code is used in order to predict the evolution of the ion beam as it acquires a velocity tilt and drifts through the background plasma to the focal plane. Space-charge, emittance, and pressure effects are especially important to consider near the simultaneous focal plane of the charge bunch because of the need to evaluate and minimize focusing aberrations and their role in the compression dynamics. Also, a PIC treatment properly describes the ion beam interaction with the background plasma and self-consistently evolves the beam's self-fields, as well as the plasma response, in situations involving incomplete (partial) charge and current neutralization. All of the simulations presented in this paper solve the electromagnetic field equations, treat all particle species as kinetic, resolve ω_{pe} and Ω_{ce} (the electron plasma and cyclotron frequencies, respectively), conserve energy to good accuracy, and include fringe $\mathbf{B}_{sol}$ fields.

A 2-D (r, z) PIC simulation for maximizing the current density achieved at the simultaneous focal plane for a given set of experimental constraints has been carried out as follows. A 400 keV K^+ beam with a 1.8 cm radius and 80 mA of beam current is initialized with a 0.2 eV transverse and longitudinal temperature (0.084 mm-mrad rms normalized emittance); these are approximately the peak parameters for an ion beam created using existing NDCX equipment. The beam is injected into the NDCX beam chamber (3.8 cm radius) in the $+z$ direction just "upstream" of the 3 cm-wide acceleration gap with an initial pulse length of 0.7 μs.

The acceleration gap of the linear induction accelerator imposes a 40% velocity tilt (defined as $\Delta v_z/v_{z,0}$) to the beam using the voltage waveform illustrated in Fig. 2. The injection timing is chosen so the beam encounters only the longitudinally focusing part of the time-dependent voltage waveform (from 200 to 900 ns in Fig. 2). The corresponding electric field in the gap region changes magnitude and
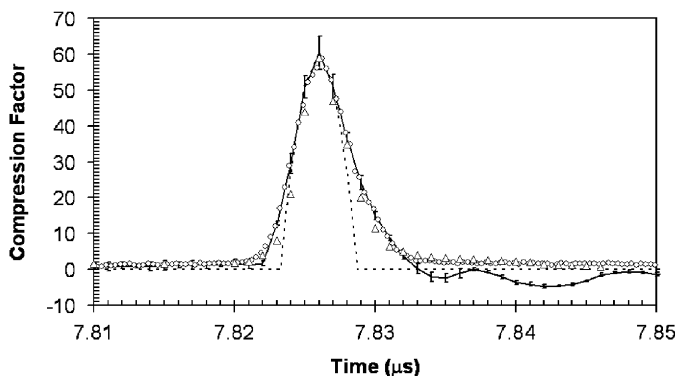

Fig. 1. Comparison of longitudinal current compression, $I(t)/I_{initial}$, at the focal plane between the experimental measurement using a fast Faraday cup (solid line with error bars), LSP simulation (open circles), kinetic model (dashed line), and hybrid model (open triangles).

direction such that it decelerates the front of the beam ($-E_z^{gap}$ from 200 to 650 ns in Fig. 2) and accelerates the back of the beam ($+E_z^{gap}$ from 650 to 900 ns in Fig. 2). After its axial velocity profile has been linearly tilted, the beam subsequently drifts through a 2.5 m plasma column filled with background plasma ($n_p^{drift} = 10^{11}\,cm^{-3}$, $T_p^{drift} = 3\,eV$).

A multi-Tesla, final-focus solenoid filled with plasma is modeled (with fringe-fields) near the end of the drift region in order to ensure that the ion beam undergoes transverse focusing to a sub-millimeter spot size coincident with the longitudinal focal plane. As the beam transversely focuses due to the $v_\theta \times B_z$ Lorentz force, the beam density increases quadratically with decreasing radius, and enough plasma must be provided to adequately satisfy $n_b \ll n_p$ for neutralization of the beam's rapidly growing charge and current density. For this reason, the density of the plasma initialized in the final-focus solenoid was chosen to be higher than the bulk plasma initialized throughout the drift region ($n_p^{focus}/n_p^{drift} \sim 10^3$) in order to accommodate the fast rise in beam density found near the simultaneous transverse and longitudinal focal plane. Fig. 3 illustrates a schematic of the NDCX geometry, from the induction accelerator to the focal plane, as modeled in the LSP simulations.

The use of a final-focus solenoid controls the effective focal length of the transverse beam compression and

thereby helps minimize the amount of high-density plasma required throughout the system. However, since the axial velocity of the beam is tilted for longitudinal compression, a wide range of beam energies enters the solenoid, resulting in aberration of the transverse focal plane. For a static $\mathbf{B}_{sol}(r, z)$, the lower-energy front of the tilted beam transversely focuses earlier in space and time, whereas the higher-energy end of the tilted beam transversely focuses later in space and time; the axial placement of the final-focus solenoid must be precisely positioned so that the longitudinal focal plane is centered on the transverse focal plane of the center of the beam, ensuring the optimal amount of simultaneous transverse and longitudinal compression. A smaller axial velocity tilt alleviates a portion of the transverse focusing aberration, but at the cost of reducing the amount of longitudinal compression.

The PIC simulations demonstrate that background plasma of sufficiently high density almost completely neutralizes the charge and current of an ion beam, facilitating large amounts of current density compression at the simultaneous focal plane. A peak beam current of 20 A with a full-width, half-maximum pulse duration of 2.3 ns is achieved at an axial location of 2.5 m "downstream" of the acceleration gap for the prescribed beam parameters and voltage waveform. The longitudinal compression factor is determined to be 250 (peak beam current normalized to the initial current). The strongest solenoid used in simulation was 150 kG in on-axis magnitude and, when properly situated at the focal plane, results in a beam spot size ($1/e$) of 0.28 mm, with a peak beam density of approximately $1.5 \times 10^{14}\,cm^{-3}$ in a background plasma of $n_p^{focus} = 3 \times 10^{14}\,cm^{-3}$ and $T_p^{focus} = 3\,eV$.

The current density of such a highly compressed charge bunch is found to increase by more than a factor of 10^5 compared to the initial current density in a focal distance of just a few meters. In particular, the associated on-axis cumulative energy deposition at the simultaneous focal plane is $5\,J\,cm^{-2}$. Fig. 4 shows the beam density profile at the time of simultaneous focus as well as the radial energy deposition profile of the beam pulse through the focal plane. In order to assess the heating capability of ion beams
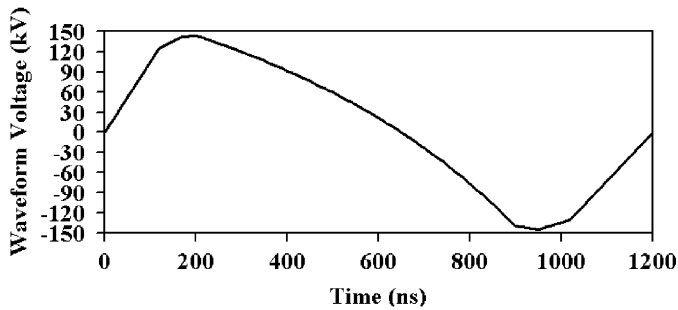

Fig. 2. The linear induction accelerator uses the voltage waveform shown in the figure in order to apply an axial velocity tilt to the ion beam as it traverses the acceleration gap region.
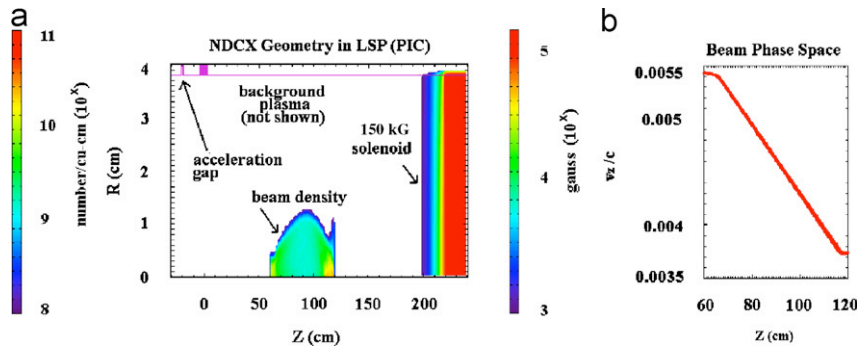

Fig. 3. (Color online) A snapshot of the LSP simulation geometry after the axial velocity tilt has been applied to the beam: (a) the model includes the acceleration gap, the ion beam density (log scale), a plasma (not shown) of density $n_p^{drift} = 10^{11}\,cm^{-3}$ extending from $z = 0$ to $z = 250\,cm$, a 150 kG final-focus solenoid (log scale) near the end of the chamber, and a plasma (not shown) of $n_p^{focus} = 3 \times 10^{14}\,cm^{-3}$ within the solenoid; and (b) the (z, v_z) phase space plot of the tilted ion beam at the location shown in (a) in normalized velocity units.
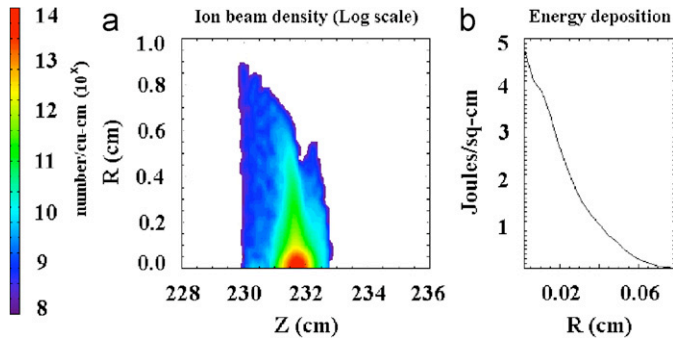
Fig. 4. (Color online) Ion beam properties at the simultaneous focal plane (within a 150 kG final-focus solenoid): (a) density (log scale); and (b) radial profile of cumulative energy deposition through the focal plane.

carrying high current densities in short pulse durations for warm dense matter applications, hydrodynamic simulations using the HYDRA code [23] are used to model the interaction of the transversely and longitudinally compressed beam with a 10% solid-density Al foam target [24]. The simulations show that the temperature of a thin (10 μm) target would reach 1.65 eV before hydrodynamic disassembly.

When the voltage waveform is nearly ideal, as it was in this optimized simulation, beam temperature effects and the finite acceleration gap geometry limit the achievable minimum pulse width at the longitudinal focal plane. Both effects play an important role in determining the upper limit of achievable current density compression when a near-ideal voltage waveform is employed. Therefore, a final pulse width of ~2 ns is likely to be near the experimentally achievable lower limit for this configuration of the NDCX device (given the ion source temperature, acceleration gap geometry, and long voltage waveform of Fig. 2). In addition, the choice of the neutralizing background plasma profiles as well as the strength and position of the final-focus solenoid are critical parameters involved in the realization of large compression factors.

3. Compression dependence on background plasma and final-focus solenoid

In Section 2, it was assumed that the 2.5 m drift chamber was entirely filled with a prescribed amount of high-density background plasma, thereby allowing quiescent beam propagation above the traditional space-charge limit as the beam focuses. Two proposed methods to provide a few meters of background plasma in the drift chamber are the use of a $BaTiO_3$ ferroelectric plasma source and a cathodic arc plasma source (CAPS). The latter requires a background solenoidal magnetic field to act as a guide for the plasma to fill the chamber by flowing along field lines, since the source is located at the "downstream" end of the NDCX device and supersonically injects plasma "upstream" into the drift region. The former does not require an external magnetic field because the plasma in the

cylindrical ferroelectric source is created at the walls and radially fills the chamber. Both types of sources are modeled in large-space-scale, long-time-scale PIC simulations in order to assess the evolution of the spatial density profiles.

The $BaTiO_3$ ferroelectric plasma source simulations were carried out in 3D in order to investigate plasma flow in azimuthally asymmetric plasma creation situations found along the source's walls, as well as in axially asymmetric plasma creation situations due to the presence of transverse diagnostic ports, which do not create plasma. Simulations indicate that asymmetric plasma creation conditions at the source's walls nevertheless result in azimuthally symmetric plasma density profiles at the time of peak on-axis n_p^{drift}. However, the peak on-axis n_p^{drift} value depends on the amount of plasma creation asymmetry at the source's walls, since more locations that do not create plasma lead to lower total plasma densities in the source. Likewise, the simulations also illustrate that the plasma will flow into the axial regions where the diagnostic ports reside by the time of peak on-axis n_p^{drift}, with a relative plasma density decrease of approximately 3 in the port locations.

The CAPS plasma source supersonically injects high-density background plasma into the drift region in the "upstream" direction from the "downstream" end of the NDCX device. The plasma is created in two off-axis locations "downstream" of the drift chamber and flows into that chamber along magnetic field lines provided by two short guide solenoids, which are placed at angles relative to a long guide solenoid used in the main drift region. 3-D PIC simulations, using the spatial magnetic field topology created by the geometry of the three solenoids, were carried out in order to study the evolution of the plasma flow provided by the plasma source. In one scenario, the coupling efficiency of plasma from the source to the drift region of the beam is 50%, since plasma drifts arising from magnetic field gradients and curvature are important.

It was also assumed in Section 2 that the final-focus solenoid is entirely filled with the requisite high-density plasma throughout the region of high magnetic field. There exists a variety of means to fill a multi-Tesla solenoid with plasma. One proposed method is to longitudinally inject the plasma with an "upstream" directed velocity into the magnetic field region from the "downstream" end of the strong magnet using a CAPS. The supersonic plasma would then fill the solenoid in a certain amount of time and the compressing ion beam would enter the final-focus solenoid from the "upstream" end. Large-space-scale, long-time-scale 2-D (r, z) PIC simulations of plasma flow into a multi-Tesla magnetic field have been performed in order to test the feasibility of such solenoidal plasma filling.

The simulations indicate that a high-field solenoid can become partially filled by an axially drifting high-density plasma in order to provide the necessary charge and current neutralization of the compressing beam, as shown in Fig. 5. In the simulations, only one-half of the solenoid's
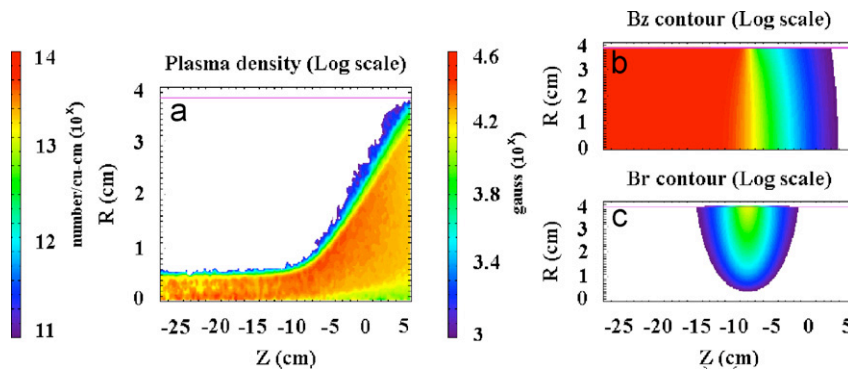
Fig. 5. (Color online) LSP simulation of longitudinal plasma injection into a 40 kG solenoid: (a) plasma density (log scale) at $t = 12\,\mu s$; (b) initial $B_z(r, z)$ contour; and (c) initial $B_r(r, z)$ contour.

axial extent is simulated and the simulation space extends from $z = -30$ to $+10$ cm. Coulomb collisions between all species were included in the model. An $Al^+ - e^-$ plasma ($n_p = 10^{13}\,cm^{-3}$, $T_p = 15\,eV$) is initialized at $z = +10$ cm with an ion directed axial velocity of $v_z^i = 4.5\,cm/\mu s$ (approximately Mach 3) from the low-field end of a 40 cm-long, 40 kG solenoid with radius 3.8 cm. After about 12 μs, the plasma flow equilibrates and fills the solenoid out to a radius of 0.6 cm, largely by flowing along magnetic field lines. Most particles are reflected away from the high-field region, but plasma particles with large enough $v_\parallel/v_\perp$ velocity component ratios are able to partially fill the 40 kG solenoid. In the process, the plasma density is compressed by nearly an order-of-magnitude, which helps to achieve the background plasma density requirements for neutralization near the simultaneous focal plane. Also, an increase in longitudinal injection velocity for the ions has the effect of increasing the radial amount of plasma fill in the solenoid. The injection velocity value used is three times larger than measured in an existing cathode-arc plasma source, however, the ratio of the injection velocity to sound speed is comparable.

We now return to the simulations carried out in the previous section to investigate whether a difference in the beam's compression is evident when the final-focus solenoid is filled with plasma only to a radius of 0.6 cm, which can be less than the beam's radius at the entrance to the solenoid, depending on the details of the charge bunch propagation. We consider this case, since an ion beam entering with a smaller radius than the fill value would not encounter a region free of plasma.

The PIC simulations described in Section 2 were repeated except with the high-density plasma present in the final-focus solenoid only to a radius of $r = 0.6$ cm. It is found that the same compression results are obtained when the final-focus solenoid is partially filled with high-density plasma compared to the fully filled case. Evidently, electrons can become trapped in the beam potential and dragged by the beam ions into the solenoid along the magnetic field lines such that quasi-neutrality is maintained in the region initially absent of plasma ($r > 0.6$ cm). In addition, neutralization of the on-axis beam

space-charge by the high-density plasma ($r < 0.6$ cm) greatly diminishes the ability of the self-fields to affect the compression, since most of the beam enters the final-focus solenoid within the plasma fill radius in an optimized configuration.

It is important to note the difference between partial-fill and no-fill final-focus solenoids located at the simultaneous focal plane. Simulations entirely lacking plasma in the region of the simultaneous focal plane show that the bulk of the plasma electrons do not sufficiently penetrate into the high-field region and the beam does not compress well, due to the very strong defocusing space-charge forces of the unneutralized beam. The space-charge potentials associated with unneutralized beam densities of interest here (in excess of $10^{13}\,cm^{-3}$) are in the kV range. In the no-fill limit, only a small population of electrons $n_e \sim n_b$ is pulled into the high-field solenoid by the beam's space-charge potential and, as the beam continues to compress, the trapped electrons also compress and therefore heat substantially. The electron temperatures associated with such a trapped population are shown in simulations to rise to 0.1–1 keV as the beam tries to focus. The beam's transverse and longitudinal focusing trajectories stagnate under such circumstances due to the strong self-fields resulting from insufficient neutralization by the hot electron population over the remaining distance to focus (> 10 cm), the beam stagnates and expands before the intended focal plane, and optimal compression factors are not realized. Fig. 6 illustrates such beam stagnation and electron heating when the simulation described in Section 2 is attempted without any neutralizing plasma initialized in the final-focus solenoid.

The strength and axial placement of the multi-Tesla final-focus solenoid are two important factors for obtaining optimal compression, since a precise $\mathbf{B}_{sol}(r, z)$ profile is responsible for the coincident transverse compression to the longitudinal focal plane, given a set of beam parameters and sufficient neutralization provided by the background plasma. Although attractive for high amounts of transverse compression, a 150 kG magnetic field which is situated at the focal plane (which also houses the target) may introduce a number of complications.

Fig. 7. Cumulative beam energy deposition profiles for the six cases reported in Table 1: (solid circle) 150 kG solenoid immersed in the focal plane; (open circle) 150 kG solenoid placed "upstream" of the focal plane; (solid triangle) 100 kG solenoid immersed in the focal plane; (open triangle) 100 kG solenoid placed "upstream" of the focal plane; (solid square) 50 kG solenoid immersed in the focal plane; and (open square) 50 kG solenoid placed "upstream" of the focal plane. All cases contained neutralizing background plasma with $n_p^{drift} = 10^{11}$ cm^{-3} and $n_p^{focus} = 3 \times 10^{14}$ cm^{-3}.
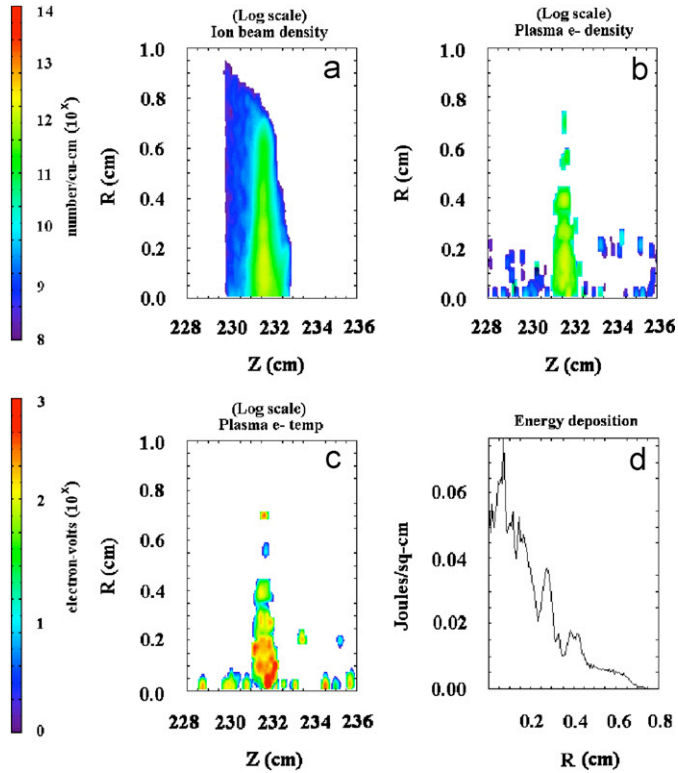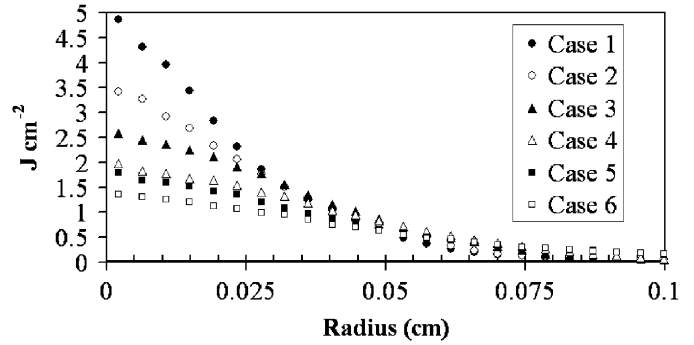
Fig. 6. (Color online) Greatly reduced compression, relative to the simulation in Section 2 (Fig. 4), occurs when the ion beam encounters a final-focus solenoid initialized without background plasma: (a) ion beam density (log scale, same as Fig. 4); (b) plasma electron density (log scale, same as Fig. 4); (c) plasma electron temperature (log scale); and (d) radial profile of cumulative beam energy deposition through the intended focal plane ($z = 232$ cm). Significant stagnation and electron heating has already taken place at the location of the intended focal plane.

Table 1
Illustrative final-focus solenoid configurations

No.	B^{pk} (kG)	B^{foc} (kG)	z^{sol} (cm)	l^{sol} (cm)	n_b^{foc} (cm^{-3})	r_b^{foc} (mm)
1	150	131	−5	16	1.5×10^{14}	0.28
2	150	10	−9	6	1.2×10^{14}	0.37
3	100	98	−5	26	9×10^{13}	0.46
4	100	4	−13	10	7×10^{13}	0.53
5	50	46	−15	40	6×10^{13}	0.49
6	50	1.5	−22	26	5×10^{13}	0.55

Therefore, the PIC simulations described in Section 2 were repeated for a variety of final-focus solenoid choices, including decreased peak magnetic field magnitudes and shifts in axial location. Simulations involving both types of change increase the achievable spot size and result in reduced energy deposition profiles and heating estimates at the simultaneous focus. The axial position of the solenoid was moved farther "upstream" in order to reduce the local magnetic field in the region of the simultaneous focal plane. The transverse compression of the beam was not as large, but sub-millimeter spot sizes were still realized. Table 1 categorizes various final-focus solenoid configurations by

peak solenoidal magnetic field strength (B^{pk}), field strength at focus (B^{foc}), axial location of the center of the solenoid relative to the focal plane (z^{sol}), total length of the solenoid (l^{sol}), peak on-axis beam density at focus (n_b^{foc}), and minimum beam radius ($1/e$) at focus (r_b^{foc}). The odd-numbered cases correspond to solenoids which are situated at the focal plane, whereas the even-numbered cases employ solenoids which do not reside at the focal plane. The cumulative beam energy deposition profiles at the simultaneous focal plane for each of the six cases are shown in Fig. 7.

In general, optimization of the beam's trajectory as it enters the final-focus solenoid plays an important role in achieving large amounts of energy deposition. In the space-charge-dominated limit, the beam's trajectory is especially sensitive to conditions involving non-neutral beam transport, such as transport from the source injector to the exit of the acceleration gap (after which the beam encounters neutralizing plasma). The finite extent of the acceleration gap creates transverse as well as axial electric fields, which act on the non-neutral beam, and is responsible for time-dependently altering the transverse trajectories of the beam ions as the longitudinal velocity tilt is applied. Therefore, the two types of focusing aberration, transverse and longitudinal, are coupled. It is desirable for the beam to have a small radius as it enters the final-focus solenoid in order to reduce transverse focusing aberration originating from the velocity tilt (see also in Section 2), as well as to minimize the amount of beam which encounters regions lacking high-density plasma. However, the time-dependent radial variation of the beam caused by the acceleration gap prevents the beam from entering the final-focus solenoid with a constant temporal radial profile. Consequently, the beam trajectory needs to be carefully selected for a given acceleration gap geometry and final-focus solenoid placement in order to balance the sources leading to decreased

compression factors and increased final spot sizes and pulse widths at focus. Both the longitudinal and transverse dynamics are important in determining the optimal compression scenario, especially in circumstances involving such highly compressed ion beams with anisotropic temperature profiles propagating in plasmas whose densities do not satisfy $n_b \ll n_p$ at all locations. The optimization sensitivity to so many beam, plasma, and external force parameters is striking.

As the beam simultaneously focuses transversely and longitudinally near the end of the drift region, the beam density can increase to values above the background plasma density if an adequate supply of background plasma is not provided, leading to a lack of charge and current neutrality. Under some circumstances, the beam compression stagnates (and optimal compression is not achieved) due to defocusing self-field forces and the plasma response to the partially neutralized intense beam, which cannot continue to propagate quiescently. Therefore, the final spot radius of the charge bunch is greatly dependent upon the electron population located in the vicinity of the focal plane.

4. Beam–plasma interaction near simultaneous focus

Provided $n_b \ll n_p$ throughout the drift region and near the focal plane, a plentiful supply of electrons is available to neutralize the charge and current of the beam ions, so the compression dynamics are mostly limited by the beam temperature and voltage waveform accuracy. In such cases, the dynamical evolution of the charge bunch can be determined exactly for a prescribed initial distribution function of the beam ions according to a recently developed kinetic formalism [18] for completely neutralized ion beams. However, the beam density can approach values of the plasma density depending on the particular experimental profiles provided for $n_p(r,t)$, especially near the simultaneous focal plane, and the assumption of complete neutralization may become invalid.

In the case of an inadequate plasma supply, the beam density approaches and surpasses the initial background plasma density during simultaneous compression, beam stagnation ensues due to self-field effects, and nonlinear beam-plasma interaction occurs. The resulting amount of current density compression achieved by the ion beam in such cases will be substantially less than the case of complete neutralization, primarily due to transverse defocusing. Moreover, the longitudinal compression deteriorates as well.

The beam–plasma interaction during simultaneous compression under conditions of inadequate neutralization by the background plasma is complicated by the presence of the external solenoidal magnetic field [25], which influences the neutralization process due to the strongly magnetized electrons. The simulations indicate that higher plasma densities are required to effectively neutralize the

beam charge in the presence of a strong magnetic field, because the plasma skin depth (c/ω_{pe}) is much larger than the electron Larmor radius (ρ_{Le}) for the parameters needed here. The length of the charge bunch decreases to within an order of magnitude of its radius at simultaneous focus, which can become comparable to the skin depth, so that charge neutralization is harder to provide for a given amount of plasma.

When local charge and current neutrality conditions are violated, strong collective excitations are generated in the plasma [26] by the beam–plasma interaction in the presence of an applied solenoidal magnetic field. The simulations illustrate that the local charge and current densities can become large in regions where n_b equals or exceeds n_p, due to an overabundance of ions, as shown in Fig. 8. The beam's transverse and axial electric self-fields grow significantly, and oppose the transverse and longitudinal focusing trajectories of the ions. As the compressing beam stagnates, the local charge and current densities become large, and the local plasma response is greatly modified by the presence of the self-fields, resulting in collective excitations in the background plasma, as well as substantial local plasma heating in some cases.
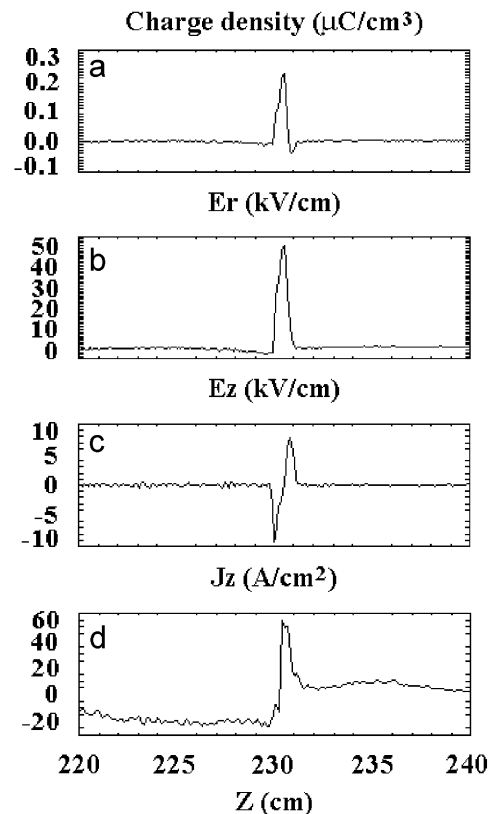

Fig. 8. Local charge and current neutrality conditions are violated when $n_b > n_p$ near the simultaneous focal plane, providing a large perturbation to the background plasma. Plots versus z of: (a) total charge density; (b) radial electric field; (c) axial electric field; and (d) axial current density. The charge density perturbation approximately satisfies $\delta_n/n_p \sim 1$. All slices are taken near the axis during stagnation of the ion beam pulse.
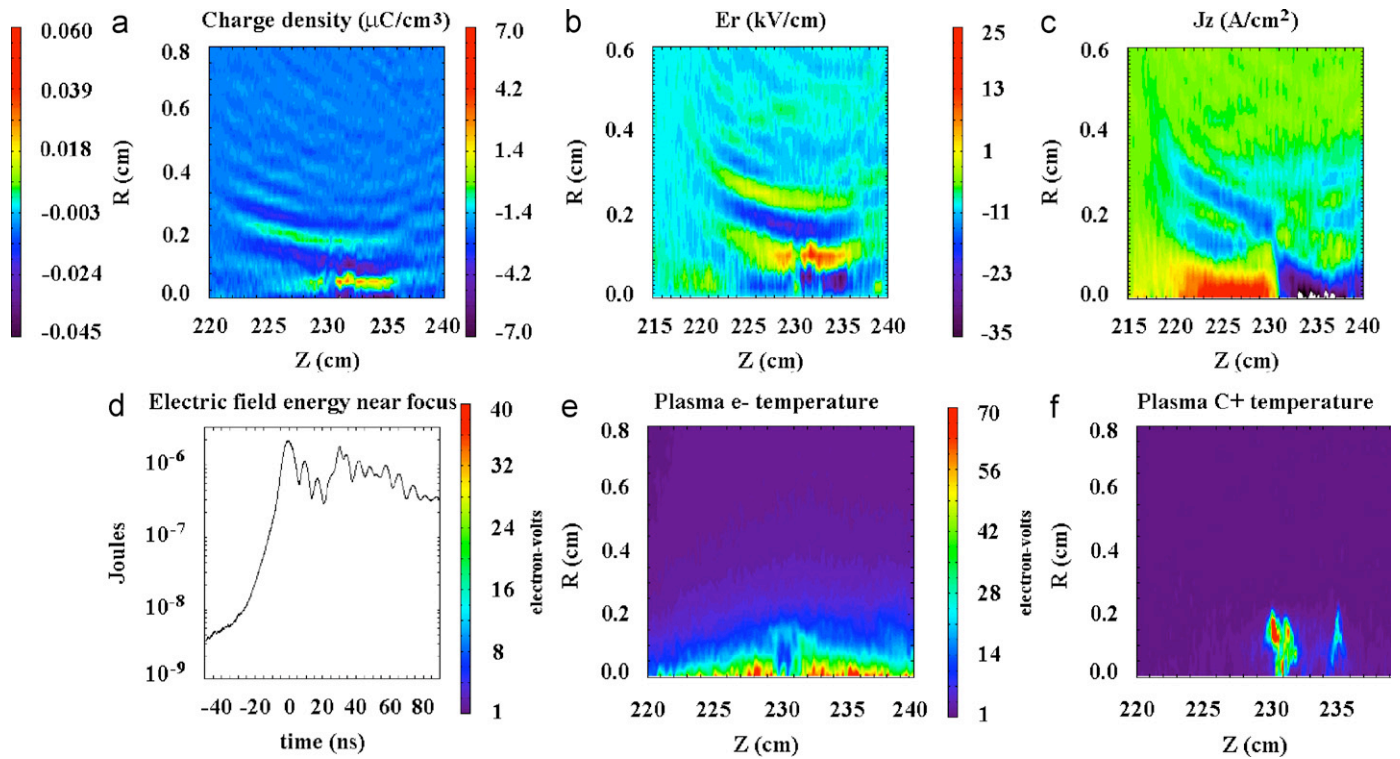
Fig. 9. (Color online) An electrostatic wave excited by the beam–plasma interaction for $n_b > n_p$ is evident as the ion beam stagnates and passes the intended focal plane. Plots in the figure show: (a) total charge density; (b) radial electric field; (c) total axial current density; (d) temporal history of electric field energy near the focal plane; (e) plasma electron e^- temperature; and (f) plasma ion temperature. The snapshots in (a), (b), (c), (e), and (f) are taken about 55 ns after beam stagnation. Time in the history plot, (d), has been rescaled so $t = 0$ corresponds to when the beam begins defocusing after stagnation.

Once the beam compression has stagnated, the beam density and self-fields cease to grow and the plasma can support strong electrostatic ($\nabla \times \delta E \approx 0$) and electromagnetic ($\nabla \times \delta E \neq 0$) excitations, due to the large charge and current density perturbations created during stagnation of the ion beam. In the simulations presented here, a strong electrostatic wave is excited by the large charge density perturbation created (shown in Fig. 8), using the beam and solenoid parameters given in Section 2, in a background plasma whose density is lower than the expected peak beam density at simultaneous focus ($n_p^{focus} = 10^{12}\,cm^{-3}$, $T_p = 1\,eV$). Fig. 9 illustrates the effects of the wave on various parameters. The wave excitation frequency is observed to be $\omega \sim 8 \times 10^8\,rad\,s^{-1}$, which lies within the range $\Omega_{ci} < \omega_{pi} < \omega \ll \omega_{pe} < \Omega_{ce}$. The wave propagates approximately perpendicular to the external $\mathbf{B}_{sol}$ in a background carbon plasma ($m_e/m_i \sim 4.5 \times 10^{-5}$) with wave vector $k_\perp \sim 6.3 \times 10^3\,m^{-1}$, and a small wave vector component parallel to the external $\mathbf{B}_{sol}$ that satisfies $k_{\parallel}/k_\perp \sim 4 \times 10^{-3}$. The wave excitation appears to be a lower hybrid wave, which can propagate with arbitrary angle relative to the external magnetic field over a broad range of plasma parameters and exhibit a resonance cone [26,27]. The solution corresponding to an electrostatic lower hybrid oscillation obtained from the cold-plasma dispersion relation which propagates at an angle θ relative to an external magnetic field is given by [28]

$$\omega^2 \sim 1/2(\omega_{pe}^2 + \Omega_{ce}^2) - 1/2[(\omega_{pe}^2 + \Omega_{ce}^2)^2 - 4\omega_{pe}^2\Omega_{ce}^2\cos^2\theta]^{1/2},$$

where $\theta = \pi/2 - \alpha$ and $\alpha \sim 4 \times 10^{-3}\,rad$, and is approximately satisfied for the parameters in these simulations. Inclusion of thermal effects does not remove the wave's ability to propagate; indeed, the wave was also observed in simulations using an increased $T_p = 10\,eV$. In fact, the background plasma ions (C^+) and electrons are both locally heated by the beam–plasma interaction up to 50 eV in this simulation, with peak temperatures reaching 400 eV near peak beam compression (stagnation).

A general analysis of nonlinear wave excitation physics during the beam–plasma interaction is difficult because of the non-equilibrium nature of a compressing charge bunch near the simultaneous transverse and longitudinal focal plane. A more refined analysis of the plasma response would need to consider corrections involving the inhomogeneous density and self-field profiles of the partially neutralized ion beam, non-uniform external magnetic field, inhomogeneous background plasma ion and electron density profiles, and thermal effects. Depending on the beam and plasma parameters, as well as the strength of the external magnetic field, a wide variety of excitations may be

generated in the background plasma by the beam–plasma interaction for the case of inadequate beam neutralization by the background plasma.

5. Conclusions

The optimization of the simultaneous transverse and longitudinal focusing of an intense ion charge bunch for a given set of experimental conditions was reported in this paper. Simulations indicate that a 400 keV K^+ ion beam can be transversely and longitudinally compressed in current density by a factor greater than 10^5 over a distance of 2.5 m. Such an intense pulse can be achieved as long as various system components are optimized; a precisely controlled voltage waveform can impart a nearly ideal axial velocity tilt to the ion beam, which can be transversely focused to the longitudinal focal plane by a strong final-focus solenoid. The background plasma must neutralize the beam's charge and current throughout the entire focusing process, otherwise the beam compression may stagnate, optimal compression may not be realized, and collective excitations may be supported in the background plasma. Therefore, compressed ion beams for use in warm dense matter experiments will require high-density plasmas in the vicinity of the focal plane. Ultimately, the beam's transverse compression is largely determined by the choice of final-focus solenoid, along with its position in the drift region and the amount of plasma provided for neutralization. When the applied axial velocity tilt is nearly linear, the longitudinal compression is largely determined by the temporal amount of the tilt and the background plasma properties. The transverse and longitudinal beam temperatures contribute to focusing aberrations in both directions, and are limiting factors for achieving small spot sizes and short pulse durations. The compression dependence on plasma temperature was also exhibited in simulations, with lower temperatures providing better neutralization. For cold, high-density plasmas in the final-focus solenoid, scattering effects may also alter the compression dynamics of the charge bunch. All of the aforementioned aspects need to be carefully considered in an experiment involving simultaneous transverse and longitudinal ion beam focusing in order to optimize the amount of current density compression (and therefore power density on target) for a given set of conditions.

Acknowledgments

References

[1] D.A. Callahan, Fusion Eng. Des. 32–33 (1996) 44.
[2] B.G. Logan, D.A. Callahan, Nucl. Intrum. Meth. Phys. Res. A 415 (1998) 468.
[3] I.D. Kaganovich, et al., Phys. Plasmas 8 (2001) 4180.
[4] I.D. Kaganovich, A.B. Sefkow, E.A. Startsev, R.C. Davidson, D.R. Welch, Effects of Finite Pulse Length, Magnetic Field, and Gas Ionization on Ion Beam Pulse Neutralization by Background Plasma, Nucl. Instrum. Meth. Phys. Res., (these proceedings).
[5] D.R. Welch, D.V. Rose, B.V. Oliver, R.E. Clark, Nucl. Instrum. Meth. Phys. Res. A 464 (2001) 134.
[6] C.H. Thoma, et al., Phys. Plasmas 12 (2005) 043102.
[7] E. Henestroza, S. Eylon, P.K. Roy, S.S. Yu, et al., Phys. Rev. ST Accel. Beams 7 (2004) 083501.
[8] P.K. Roy, S.S. Yu, et al., Phys. Plasmas 11 (2004) 2890.
[9] P.K. Roy, et al., Nucl. Instrum. Meth. Phys. Res. A 544 (2005) 255.
[10] D.R. Welch, D.V. Rose, S.S. Yu, J.J. Barnard, C.L. Olson, Nucl. Instrum. Meth. Phys. Res. A 544 (2005) 236.
[11] N. Christofilos, et al., Rev. Sci. Instrum. 35 (1964) 886.
[12] P.K. Roy, S.S. Yu, et al., Phys. Rev. Lett. 95 (2005) 234801.
[13] P.K. Roy, S.S. Yu, E. Henestroza, et al., Neutralized Drift Compression Experiments (NDCX) for High Intensity Ion Beams, Nucl. Instrum. Meth. Phys. Res., (these proceedings).
[14] A.B. Sefkow, et al., Phys. Rev. ST Accel. Beams 9 (2006) 052801.
[15] A.B. Sefkow, et al., Proceedings of the 2005 Particle Accelerator Conference, (2005) 3765.
[16] A.B. Sefkow, R.C. Davidson, Phys. Rev. ST Accel. Beams 9 (2006) 090101.
[17] H. Qin, R.C. Davidson, J.J. Barnard, E.P. Lee, Nucl. Instrum. Meth. Phys. Res. A 544 (2005) 255.
[18] R.C. Davidson, H. Qin, Phys. Rev. ST Accel. Beams 8 (2005) 064201.
[19] P.A. Seidl, et al., Plans for Neutralized Drift Compression Experiments and Initial Results from Solenoid Transport, Nucl. Instrum. Meth. Phys. Res., (these proceedings).
[20] D.R. Welch, et al., Integrated Simulation of an Ion-Driven Warm Dense Matter Experiment, Nucl. Instrum. Meth. Phys. Res., (these proceedings).
[21] LSP is a software product of ATK Mission Research, Albuquerque, NM 87110.
[22] T.P. Hughes, S.S. Yu, R.E. Clark, Phys. Rev. ST-Accel. Beams 2 (1999) 110401.
[23] M.M. Marinak, et al., Phys. Plasmas 8 (2001) 2275.
[24] J.J. Barnard, et al., Theory and Simulation of Warm Dense Matter Targets, Nucl. Instrum. Meth. Phys. Res., (these proceedings).
[25] I.D. Kaganovich, E.A. Startsev, R.C. Davidson, D.R. Welch, Nucl. Instrum. Meth. Phys. Res. A 544 (2005) 383.
[26] T.H. Stix, Waves in Plasmas, Springer, New York, 1992.
[27] R.K. Fischer, R. Gould, Phys. Fluids 14 (1971) 857.
[28] E.M. Lifshitz, L.P. Pitaevskii, Physical Kinetics, Pergamon Press, Oxford, 1981.